Iron isotopes constrain the pathways and formation mechanisms of terrestrial oxide concretions: A tool for tracing iron cycling on Mars?

Marjorie A. Chan*
Department of Geology & Geophysics, University of Utah, 719 WBB, 135 S. 1460 E., Salt Lake City, Utah 84112, USA

Clark M. Johnson*
Brian L. Beard*
Department of Geology and Geophysics, University of Wisconsin, 1215 W. Dayton St., Madison, Wisconsin 53706, USA

John R. Bowman*
W.T. Parry*
Department of Geology & Geophysics, University of Utah, 719 WBB, 135 S. 1460 E., Salt Lake City, Utah 84112, USA

ABSTRACT

New iron isotope data document open-system formation of terrestrial iron oxide concretions and the potentially important role of iron-reducing bacteria in mobilizing iron. These terrestrial insights can provide valuable models for understanding extraterrestrial hematite spherules and their diagenetic history at Meridiani Planum, Mars. Whole-rock samples of Jurassic Navajo Sandstone host rock have $\delta^{56}Fe$ values near 0 per mil (‰), whereas concretions typically have negative $\delta^{56}Fe$ values. Negative $\delta^{56}Fe$ values can be explained by complete oxidation and precipitation from aqueous fluids that had $\delta^{56}Fe$ values of −0.5‰ to −1.5‰. The low $\delta^{56}Fe$ values for the majority of concretions overlap those of $Fe(II)_{aq}$ and reactive ferric oxides in modern marine sediments where iron-reducing bacteria are actively cycling Fe, suggesting that Fe mobilization in the Navajo Sandstone occurred through bacterial reduction of Fe oxides. Variations in $\delta^{56}Fe$ values support an open-system model of concretion formation where Fe is recycled via different chemical reactions involving reduction, mobilization, and precipitation. If the Mars concretions formed in a similarly open system during Fe mobilization and precipitation, their $\delta^{56}Fe$ values should also deviate from $\delta^{56}Fe = 0$, dependent upon the pathway, but positive $\delta^{56}Fe$ values would be expected for oxides in the absence of a role for microbial redox cycling.

Keywords: iron isotopes, concretion, hematite, diagenesis, Mars.

INTRODUCTION

Concretions are concentrated masses of mineral cements that are typically spherical, and they are very common and widespread in sedimentary rocks throughout the geologic record (e.g., Seilacher, 2001). Remarkably, the National Atmospheric and Space Administration (NASA) *Opportunity* rover discovered small hematite spherules in Meridiani Planum on Mars (dubbed "blueberries") that have been interpreted as concretions (Squyres et al., 2004; Herkenhoff et al., 2004; Christensen et al., 2004). Iron oxide concretions on both Mars and Earth are valuable records of diagenetic, postdepositional changes in sedimentary units because they preserve evidence of ancient groundwater flow (Chan et al., 2004, 2005; Ormö et al., 2004; McLennan et al., 2005), fluid-rock interactions, element cycling, and the presence of redox boundaries. The concretions typically have spherical morphologies.

The Jurassic Navajo Sandstone exposed in southern Utah contains abundant, diverse, and well-documented examples of Fe oxide (e.g., hematite and goethite) concretions (e.g., Utah "marbles") that have morphological similarities to the Mars "blueberries" in the deposits of Meridiani Planum (Chan et al., 2004, 2005). Although no single terrestrial analog is likely to be a perfect match for all the chemical and physical traits of sulfate mineralogy and Fe oxide concretions on Mars, the sediment-hosted Navajo concretions offer a natural, terrestrial laboratory that provides insights into the Meridiani Planum deposits. In this contribution, we present new Fe isotope data that allow us to constrain the Fe sources and pathways involved in concretion formation. These data document the open-system conditions that were required for concretion formation, the important role of hydrocarbons or Fe-reducing bacteria in mobilizing Fe, and the isotopic signatures of oxidation and precipitation at redox boundaries. These results provide insight into Fe mobility and redox transformations in terrestrial environments, and potentially constrain the range in Fe isotope signatures that may be found in oxide concretions on Mars in future in situ measurements or those obtained by sample-return missions.

IRON ISOTOPE GEOCHEMISTRY

Iron isotope geochemistry is a rapidly growing field, where it is now known that measurable isotopic fractionations occur in both high- and low-temperature environments (e.g., Welch et al., 2003; Beard and Johnson, 2004; Johnson et al., 2004; Dauphas and Rouxel, 2006). Some of the largest Fe isotope fractionations occur in low-temperature systems (<100 °C) during redox transformations, but only under conditions where separation of isotopically distinct Fe pools may occur (Johnson and Beard, 2006). For example, partial oxidation of aqueous Fe(II) generally leads to ferric Fe oxide or hydroxide precipitates that have higher $^{56}Fe/^{54}Fe$ ratios than the initial aqueous Fe(II). Complete oxidation, however, such as might occur when $Fe(II)_{aq}$

*E-mails: chan@earth.utah.edu; clarkj@geology.wisc.edu; beardb@geology.wisc.edu; bowman@earth.utah.edu; parry@earth.utah.edu.

encounters atmospheric O_2, or during weathering of Fe(II)-bearing igneous or metamorphic rocks, will produce ferric oxides or hydroxides that have essentially the same Fe isotope composition as the initial Fe(II) because oxidation ran to completion. This effect is well illustrated for surface weathering products, including suspended river loads, aerosols, and ferric Fe-rich clastic rocks that have low organic carbon or carbonate contents, all of which have Fe isotope compositions that are closely similar to those of the average crust (Beard et al., 2003b).

We report Fe isotope compositions using standard δ notation as the deviation in $^{56}Fe/^{54}Fe$ ratio of a sample relative to a reference reservoir, in units of parts per thousand, or per mil (‰):

$$\delta^{56}Fe = [(^{56}Fe/^{54}Fe_{sample})/(^{56}Fe/^{54}Fe_{reference}) - 1] \times 10^3,$$

where $^{56}Fe/^{54}Fe_{reference}$ is taken as the average of igneous rocks (Beard et al., 2003a). On the igneous rock scale, the IRMM-014 standard produces a $\delta^{56}Fe$ value of −0.09‰. The total spread in $\delta^{56}Fe$ values of terrestrial samples is ~4–5‰, and typical analytical precisions are ±0.05 to ±0.10‰ (2σ). Following standard convention, we describe the Fe isotope fractionation between two phases A and B as:

$$\Delta^{56}Fe_{A-B} = \delta^{56}Fe_A - \delta^{56}Fe_B.$$

This may be related to the Fe isotope fractionation factor α_{A-B} through the approximation:

$$10^3 \times \ln \alpha_{A-B} \approx \Delta^{56}Fe_{A-B}.$$

Details on chemical separation and mass analysis methods are in Beard et al. (2003a) and Albarède and Beard (2004).

CONCRETION GENESIS

The porous and permeable characteristics of the Navajo Sandstone provide favorable conditions for the formation of Fe oxide concretions (Chan et al., 2004, 2005). The well-sorted, eolian quartz arenite (Beitler et al., 2005) has effective porosity that averages ~17% (Cordova, 1978) and permeability up to 1 Darcy (Lindquist, 1988). Iron oxide mineralization can be summarized as a three-step process of diagenesis, which critically includes groundwater flow (Chan et al., 2000, 2004, 2005; Chan and Parry, 2002; Beitler et al., 2003, 2005). Diagenetic temperatures <100 °C are inferred based on an estimated burial depth of 2 km (Beitler et al., 2005) and mineralogical evidence (summarized in Chan et al., 2000), as well as supporting studies on the thermal burial history and uplift

of the Colorado Plateau (Dumitru et al., 1994; Nuccio and Condon, 1996).

Iron Sources

Red Navajo sandstones (Fig. 1A) contain an average of 0.53 ± 0.34 wt% Fe_2O_3 (1 SD) distributed as thin Fe oxide films that coat individual sand grains (Beitler et al., 2005). This iron is likely to have been derived from detrital Fe-bearing silicate minerals within the sandstone during early weathering and diagenesis. Disseminated precipitation of this early diagenetic Fe oxide occurred shortly after deposition or during early burial via interaction with meteoric waters. In terms of expected Fe isotope compositions for these early Fe oxides, they probably had $\delta^{56}Fe$ values near zero, similar to the igneous rock baseline that characterizes bulk continental crust, including low organic carbon (C_{org}) or carbonate (C_{carb}) contents, clastic sedimentary rocks, and sandstones that are rich in disseminated ferric Fe oxide cements (Beard et al., 2003b; Beard and Johnson, 2004; Yamaguchi et al., 2005; Johnson and Beard, 2005, 2006).

Iron Mobilization

After burial, reduced fluids containing hydrocarbons derived from underlying units are thought to have flowed up preferential pathways such as faults and through the porous sandstone (Chan et al., 2000). Mobilization of the early oxides is envisioned to have occurred through reductive dissolution and transport as Fe(II)$_{aq}$, leaving bleached, white sandstone (Fig. 1B). These bleached zones can be quite extensive, on the order of hundreds of square kilometers (Beitler et al., 2003). Bleached sandstones contain an average of 0.36 ± 0.26 wt% Fe_2O_3 (1 SD) as Fe oxide (Beitler et al., 2005). Based on total Fe contents of red and bleached sandstones, up to 30% of the Fe was removed. Reactions between hydrocarbons and ferric oxide may be expressed through reduction of Fe coupled with oxidation of organic matter as:

$$CH_2O + 2Fe_2O_3 + 8H^+ \rightarrow CO_2 + 5H_2O + 4Fe^{2+}$$
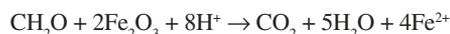
(e.g., Chan et al., 2000). The same reaction is applicable to reduction of ferric oxides or hydroxides by dissimilatory iron-reducing bacteria (DIRB) (e.g., Nealson and Saffarini, 1994). At temperatures below 120 °C, Fe(III) reduction by organic matter does not occur in the absence of DIRB (Lovley et al., 1991).

Iron isotopes are fractionated during reduction of Fe(III) oxides or hydroxides by DIRB, where Fe(II)$_{aq}$ has $\delta^{56}Fe$ values that are 1–3‰ lower than the initial ferric oxide or hydroxide

(Beard et al., 1999, 2003a; Icopini et al., 2004; Johnson et al., 2002, 2005; Crosby et al., 2005). Low-$\delta^{56}Fe$ Fe(II)$_{aq}$ is balanced by a reactive Fe(III) layer on the oxide or hydroxide mineral surface that has high $\delta^{56}Fe$ values, indicating that these minerals are dissolved incongruently by DIRB (Crosby et al., 2005). The low $\delta^{56}Fe$ fingerprint of Fe(II)$_{aq}$ that is produced by DIRB has been found in Fe(II)-rich pore waters in modern marine sediments (Severmann et al., 2006; Berquist and Boyle, 2006), and low $\delta^{56}Fe$ ferric Fe oxides in modern marine environments have been ascribed to precipitation of DIRB-produced low $\delta^{56}Fe$ Fe(II)$_{aq}$ (Severmann et al., 2006; Staubwasser et al., 2006). The Fe isotope effects of abiotic reduction of ferric oxides or hydroxides by hydrocarbons are not known, and they likely depend on the dissolution mechanism; congruent dissolution is unlikely to produce any Fe isotope fractionation (Johnson et al., 2004), but formation of a new phase or reactive surface layer during incongruent dissolution may potentially produce an Fe isotope fractionation.

Although the form and occurrence of the Navajo Sandstone concretions are strikingly similar to the small, spherical "blueberry" hematite concretions (Figs. 1F–1H) in Meridiani Planum, the mechanisms by which Fe was mobilized may have been distinct. For example, Fe in the Mars system was probably mobilized through dissolution of primary silicates in basaltic rocks by acidic solutions (e.g., Morris et al., 2005). If this Fe mobilization occurred under reducing conditions, where aqueous Fe was largely Fe(II), no Fe isotope fractionation would be expected because no redox change would occur. Partial dissolution of silicates by organic ligands under oxic conditions can produce aqueous Fe(III) that has relatively low $\delta^{56}Fe$ values (Brantley et al., 2001, 2004), although significant fractionations have only been observed at very low extents of dissolution (≤1%).

Concretion Precipitation

Precipitation of terrestrial concretions is thought to occur when Fe(II)-bearing (reduced) fluids intersected oxidizing groundwaters, where oxidation of Fe at near-neutral pH would produce immediate precipitation of Fe oxide at the mixing interface (Von Gunten and Schneider, 1991). Precipitation of Fe oxide would be concentrated within a spatially limited reaction front corresponding to this mixing interface. Concretions that precipitate within such a reaction front are commonly spheroidal in shape (Figs. 1C–1E). The average Fe concentration in the Fe oxide cemented concretions is 15.12 ± 9.99 wt% Fe_2O_3 (1 SD) (Beitler et al., 2005),
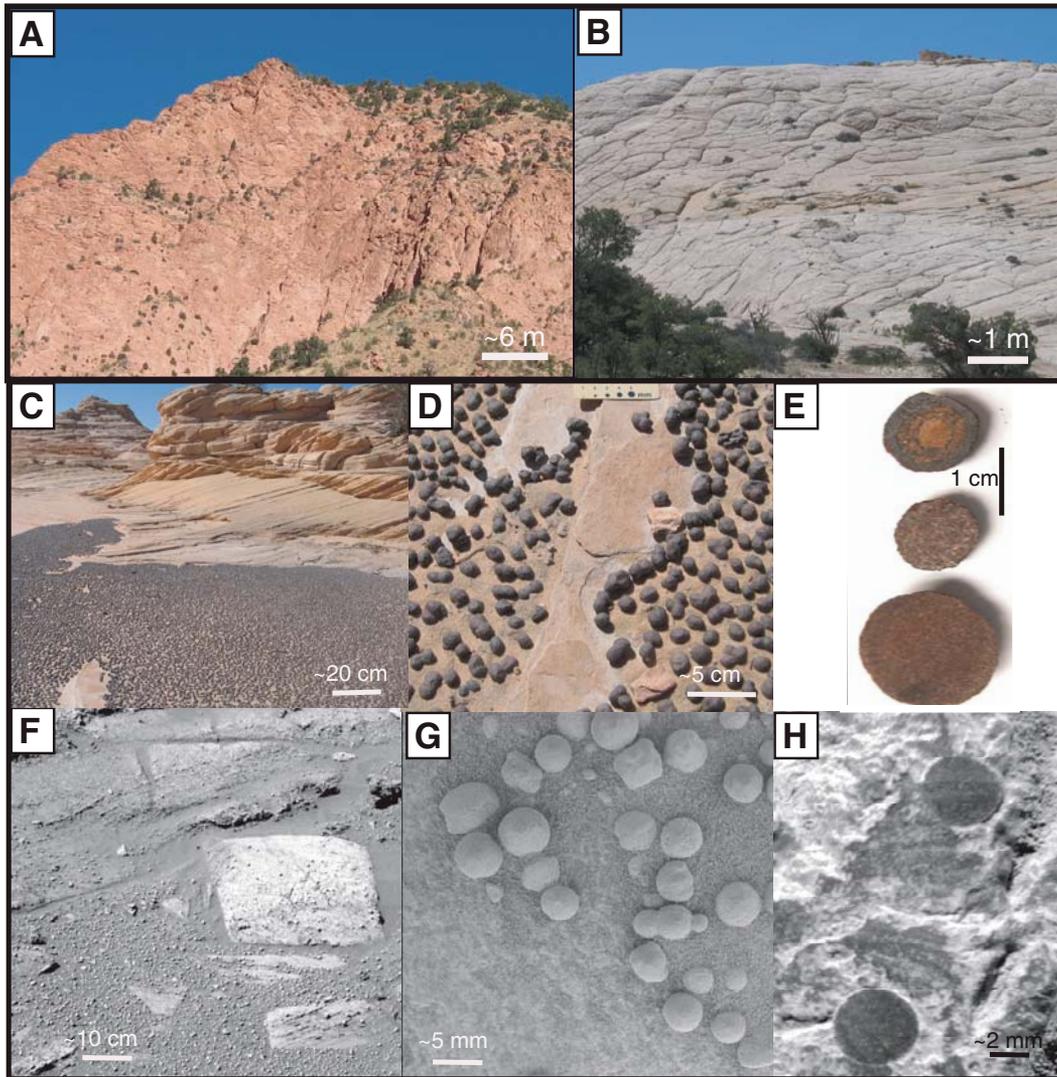
Figure 1. Example Navajo Sandstone samples analyzed with field context pictures. Whole-rock δ^{56}Fe values were measured from (A) red, original sandstones (locality 4, Fig. 2), and (B) white, bleached sandstones (locality 9, Fig. 2). (C–E) Row of terrestrial concretion images (concretion diameters typically ≥1 cm) shows in situ and weathered distributions as well as geometries (e.g., joined forms) and structures. (F–H) Row of Mars images shows hematite blueberries (averaging <0.5 cm in diameter, Squyres et al., 2004), and are comparable to terrestrial concretions. Mars images courtesy of NASA/JPL/Cornell.

where other constituents are largely SiO_2 (avg. of 77.3 wt%) and Al_2O_3 (avg. of 2.2 wt%). Age determinations of related mineralization (Chan et al., 2001) suggest that some precipitation occurred ca. 25 Ma, but mineralization appears to have been episodic and may have included older or younger events.

The Fe isotope compositions produced during oxidation and precipitation will depend upon the extent of coupled oxidation-precipitation and the degree to which precipitation occurs under equilibrium conditions (Beard and Johnson, 2004; Johnson and Beard, 2006). Partial oxidation of $Fe(II)_{aq}$ to $Fe(III)_{aq}$, followed by complete precipitation of $Fe(III)_{aq}$ to ferric oxides or hydroxides should produce δ^{56}Fe values for the ferric Fe precipitates that are ~1–3‰ higher than those of the initial $Fe(II)_{aq}$; the smaller fractionations are associated with a significant kinetic fractionation upon precipitation, whereas the maximum 3‰ fractionation

occurs when precipitation occurs slowly under equilibrium conditions. In contrast, complete in situ oxidation and precipitation should produce δ^{56}Fe values that are identical to those of the initial $Fe(II)_{aq}$, which would allow the oxide concretions to be used as proxies for the Fe isotope compositions of the precursor aqueous Fe(II).

$Fe(II)_{aq}$ oxidation and precipitation of the Martian hematite concretions are thought to have occurred upon oxidation in a highly reactive chemical environment that included formation of evaporite and sulfate minerals (McLennan et al., 2005; Tosca et al., 2005). In both the Mars and terrestrial systems, however, the Fe isotope fractionations produced during oxidation would be expected to be similar, given the fact that generally similar fractionations are observed in a wide variety of oxidative pathways, including biological and abiological systems (Bullen et al., 2001; Croal et al., 2004; Balci et al., 2006). We therefore expect that the key component in

determination of the Fe isotope compositions of concretions on Mars or Earth is the mechanism by which Fe was initially mobilized.

RESULTS

We analyzed representative samples from 16 localities of Jurassic Navajo Sandstone and 2 localities of Jurassic Entrada Sandstone across an ~400 km traverse in southern Utah (Fig. 2). These included whole-rock samples of original red host sandstone (Fig. 1A) and bleached sandstone (Fig. 1B). Whole-rock samples where color, textural, and field characteristics indicated that no late secondary Fe mobilization occurred have δ^{56}Fe values that lie within 0.2‰ of zero (avg. δ^{56}Fe = +0.04‰), the same range observed in low-C and low-S clastic sedimentary rocks that have not undergone significant anoxic diagenesis (Table DR1[1]; Fig. 3) (Beard and Johnson, 2004; Johnson and Beard, 2006). Bleached
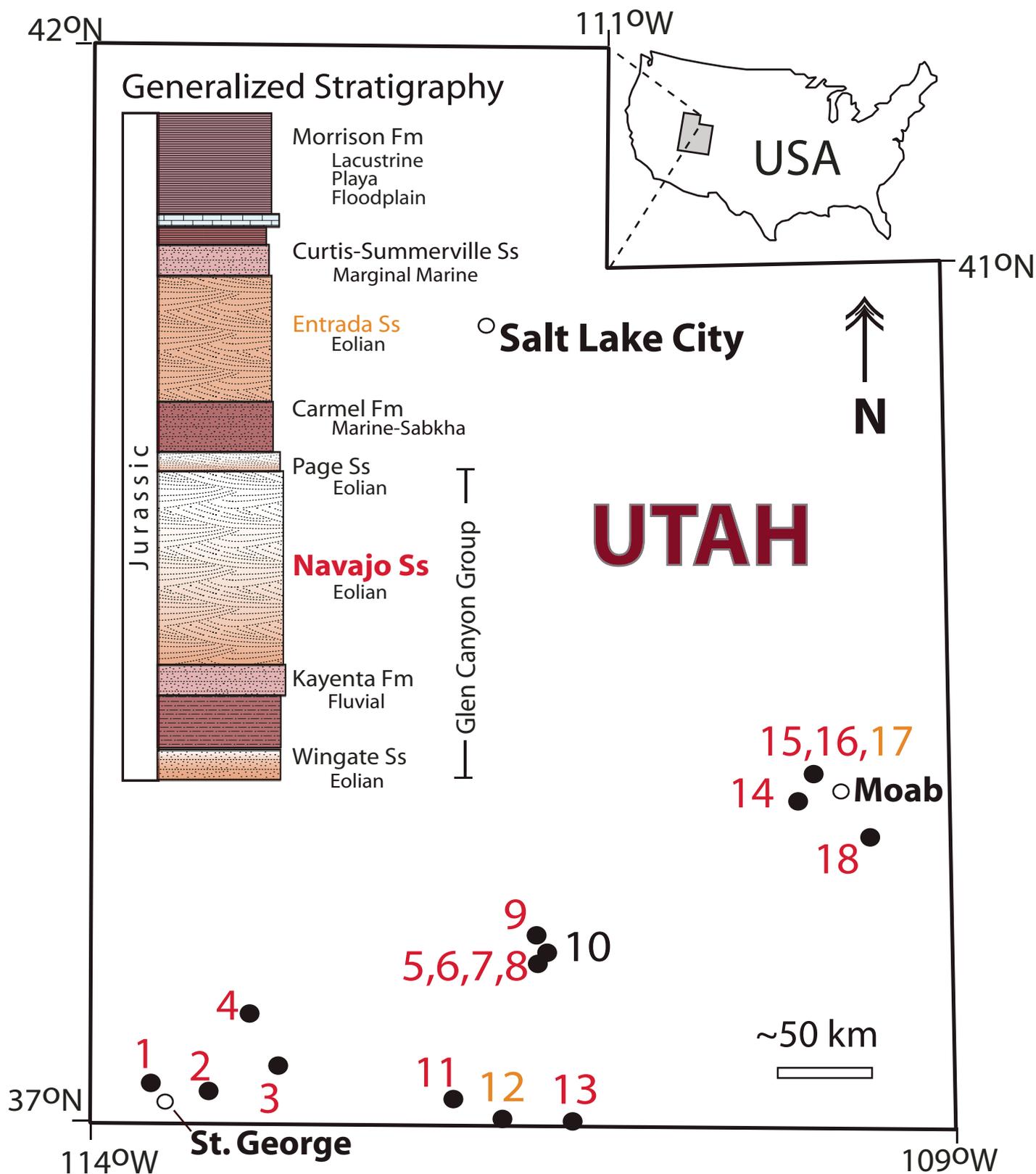
Figure 2. Localities of Jurassic sampling for Fe isotope analyses: 1—Snow Canyon, 2—Sand Hollow, 3—Zion National Park, 4—Cedar City, 5–10—Grand Staircase Escalante National Monument, 11–13—Lake Powell area, and 14–18—Moab area. All samples are from the Lower Jurassic Navajo Sandstone (Ss) except for localities 12 and 17, which are from the Middle Jurassic Entrada Sandstone. Generalized stratigraphic column is at left (modified after Chan et al., 2005).

rocks that have lost Fe have a similar range in δ^{56}Fe values, although their average is slightly higher than zero. One sample that is enriched in secondary oxides has a distinctly lower δ^{56}Fe value of −0.6‰.

Iron oxide concretions have a large range of δ^{56}Fe values from +0.9‰ to −2.0‰. The most remarkable characteristic of the concretion data is that most samples have negative δ^{56}Fe values, which is generally unexpected for oxide minerals, which would be enriched in ^{56}Fe/^{54}Fe based on Fe isotope fractionation factors (Beard and Johnson, 2004). Comparison of δ^{56}Fe values for individual concretions with whole-rock samples from the same locality generally show large isotopic contrasts, up to 1.5‰, which provides strong support for a model in which Fe was mobilized, oxidized, and precipitated in an open, fluid-rich system. There is no systematic correlation between δ^{56}Fe values and oxide mineralogy (hematite or goethite). There are, however, sometimes significant variations in δ^{56}Fe values (up to 0.8‰) within individual concretions. In several cases, the interiors of concretions have higher δ^{56}Fe values than the rims (Fig. 3; Table DR1, Fig. DR1 [see footnote 1]), but reverse zoning is also present.

DISCUSSION

The negative δ^{56}Fe values for most of the oxide concretions coupled with the wide range in these values demonstrate that they did not form by simple, closed-system remobilization of Fe from earlier diagenetic oxides, but instead formed in an open system. Congruent dissolution of early diagenetic oxide minerals, followed by complete oxidation and precipitation in a closed system, would produce little change in δ^{56}Fe values from their initial near-zero values. In principle, Fe oxides that have moderately negative δ^{56}Fe values of −0.5‰ to −1.5‰ may be produced through oxidation and precipitation from an Fe(II)-bearing fluid that has a δ^{56}Fe value of zero, but only under very special conditions. Assuming a Rayleigh process, the negative δ^{56}Fe values for the majority of oxide concretions can only be produced by first oxidizing ~70% to ~90% of the Fe(II)$_{aq}$ initially present (that had an initial δ^{56}Fe value of zero), and then selectively incorporating the last few percent of

Figure 3. Summary of measured δ^{56}Fe values from different Jurassic sandstone samples relative to sample locality (Fig. 2). Whole-rock samples are shown in blue squares. Concretion samples are shown in red circles. I—inner portion of concretion sample, R—rim of concretion sample. Also shown is the range in δ^{56}Fe values for low-C and low-S clastic sedimentary rocks (light-green band) that reflects Fe(III)-rich weathering products (Beard et al., 2003b; Yamaguchi et al., 2005), which should represent the range in δ^{56}Fe values of the early diagenetic Fe(III) oxides in the Jurassic sandstones. Vertical dashed line is the average of igneous rocks (Beard et al., 2003a).

---

[1]GSA Data Repository item 2006236, Figure DR1, original isotopic traverse measurements of concretions (rim to interior), and Table DR1, original isotopic measurements of all data samples with description of the locality (keyed to Figure 2) and mineralogy, is available online at www.geosociety.org/pubs/ft2006.htm, or on request from editing@geosociety.org or Documents Secretary, GSA, P.O. Box 9140, Boulder, CO 80301-9140, USA.
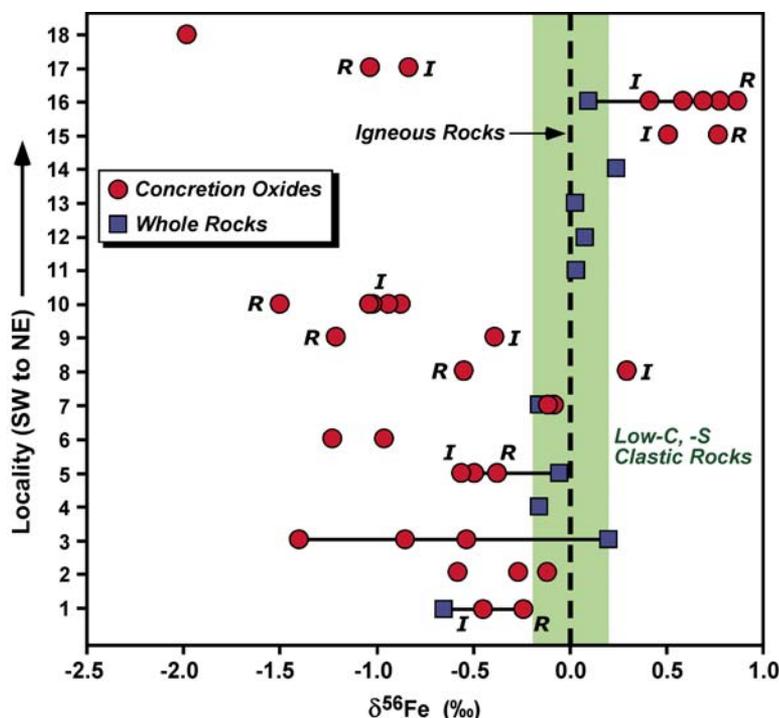
the *incrementally produced* oxide into the concretions (Fig. 4). This scenario seems unlikely for several reasons. The geological and geochemical evidence for the terrestrial model supports precipitation of Fe oxide at a reaction front produced by a mixing interface between reduced and O$_2$-rich groundwater masses. If the Fe oxide was precipitating by a Rayleigh process at this interface, the great majority of the mass of the iron oxide present would have δ^{56}Fe values significantly above 0‰ (Fig. 4). The opposite is observed; most concretions have negative δ^{56}Fe values (Table DR1, see footnote 1). Further, the terrestrial model appears to have operated at near-neutral pH conditions based on several geochemical characteristics: adsorbed species Zn, Co, Ni, As, V, and U that imply pH 6–8 for precipitation of Fe oxides (Beitler et al., 2005); co-existence of kaolinite and illite (Chan et al., 2000); and reasonable values of K$^+$ in solution (0.001 M) that imply pH ~ 6. At pH conditions of 6–8, oxidation will tend to run to completion at the reaction front where reduced fluids encounter O$_2$-rich fluids. In such a scenario, selective incorporation of a narrow range of late-stage

oxide products (e.g., Rayleigh process) into the concretions is not realistic.

Busigny and Dauphas (2006) analyzed several goethite-cemented concretions from the Navajo Sandstone in a few limited locality areas of southern Utah and suggested that negative δ^{56}Fe values measured in the concretions could be explained by evolution of the fluid composition through successive precipitation (e.g., Rayleigh process) and/or adsorption of Fe. We regard the Rayleigh process as an unlikely mechanism for the reasons presented in the preceding paragraph. Moreover, our δ^{56}Fe data on a broad range of concretion mineralogy types (many with complex layering and different δ^{56}Fe core-to-rim trends) from different reaction fronts spanning a much larger regional area lead us to favor other models that involve open diagenetic systems and the potential role of Fe(III)-reducing bacteria.

As it seems more likely that the oxide concretions were produced by complete or near-complete oxidation of Fe(II)$_{aq}$ as reduced fluids encountered O$_2$-rich zones, it is more appropriate to consider the *integrated* Fe oxide isotopic

compositions (Fig. 4). In this case, however, the integrated Fe oxide can have $\delta^{56}Fe$ values no lower than that of the initial fluid (Fig. 4). Hence, the negative $\delta^{56}Fe$ values of $-0.5\permil$ to $-1.5\permil$ for the majority of oxide concretions is best explained by oxidation, followed by precipitation, of $Fe(II)_{aq}$ that had initial $\delta^{56}Fe$ values that were negative. An end-member case would be one where the $\delta^{56}Fe$ values of the oxide concretions are a direct proxy for the $\delta^{56}Fe$ values of $Fe(II)_{aq}$, which would require complete oxidation and precipitation. Alternatively, partial oxidation, but complete precipitation, may explain the data. For example, assuming an initial $\delta^{56}Fe$ value of $-2.0\permil$ for $Fe(II)_{aq}$, ~50%–100% oxidation may produce the range in Fe isotope compositions for the oxide concretions that have negative $\delta^{56}Fe$ values (Fig. 4). Alternatively, the oxide concretions that have moderately negative $\delta^{56}Fe$ values of ~$-0.5\permil$ could be explained by ~100% oxidation and precipitation of $Fe(II)_{aq}$ that had an initial $\delta^{56}Fe$ value of ~$-0.5\permil$. The few concretions that have positive $\delta^{56}Fe$ values may be explained by ~50% to ~80% oxidation of $Fe(II)_{aq}$ that had an initial $\delta^{56}Fe$ value of zero, again using the *integrated* Fe oxide compositions (Fig. 4). We conclude that the majority of oxide concretions were formed through complete or near-complete oxidation of $Fe(II)_{aq}$ that initially had negative $\delta^{56}Fe$ values, perhaps averaging ~$-1.0\permil$, but ranging from ~0.0‰ to ~$-1.5\permil$.

Origin of Low $\delta^{56}Fe$ Aqueous Fe(II)

A number of processes may produce $Fe(II)_{aq}$ that has negative $\delta^{56}Fe$ values. Approximately 30%–70% oxidation of $Fe(II)_{aq}$ that had an initial $\delta^{56}Fe$ value of zero can, in principle, produce moderately negative $\delta^{56}Fe$ values in the remaining $Fe(II)_{aq}$ of ~$-0.5\permil$ to ~$-1.5\permil$ (Fig. 4). Such a model, however, requires two stages of oxidation and precipitation to explain the negative $\delta^{56}Fe$ values for the majority of oxide concretions: an initial partial oxidation step to produce low $\delta^{56}Fe$ $Fe(II)_{aq}$, separation of $Fe(II)_{aq}$ from the initial oxide precipitates, followed by further oxidation (and precipitation) at the site of concretion formation. The core-to-rim variations in Fe isotope compositions for a number of oxide concretions (Fig. 3) provide some evidence for changing $\delta^{56}Fe$ values of $Fe(II)_{aq}$ during concretion formation, but these changes are most likely to have occurred at the site of concretion formation, rather than on a regional scale, as would be required in a "two-step" oxidation model.

It has been proposed that sorption of $Fe(II)_{aq}$ to Fe oxides may produce low $\delta^{56}Fe$ values in the remaining $Fe(II)_{aq}$ (Icopini et al., 2004; Teutsch et al., 2005), but such proposals have been inferred from laboratory or field experiments that did not measure the sorbed Fe(II) directly. In contrast, Crosby et al. (2005) directly measured the $Fe(II)_{aq}$–$Fe(II)_{sorbed}$ fractionation and found that this fractionation was small, between $-0.3\permil$ (hematite) and $-0.8\permil$ (goethite). At pH > 7, where the proportion of sorbed Fe(II) onto oxide minerals is at a maximum (e.g., Jeon et al., 2001), such a small isotopic fractionation would only be expressed at very low $Fe(II)_{aq}$ contents, and even under these conditions, the effect would be only several tenths per mil. Under mild to strong acidic conditions (pH < 6), the very low proportion of sorbed Fe(II) eliminates sorption as a mechanism for producing significant Fe isotope changes in $Fe(II)_{aq}$, contrary to the suggestion of Balci et al. (2006). These considerations therefore make it very unlikely that sorption of Fe(II) to Fe oxide minerals is an explanation for the generally low $\delta^{56}Fe$ values that are inferred for the $Fe(II)_{aq}$ that was the source for the oxide concretions.

Evidence for Fe(III)-Reducing Bacteria

The range in $\delta^{56}Fe$ values estimated for $Fe(II)_{aq}$ that was the source of Fe for the Navajo concretions overlaps that measured for active diagenetic systems, including modern marine sediments (Fig. 4). Severmann et al. (2006) noted that porewater Fe(II) in suboxic sections of modern marine sediments (California margin) where DIRB are likely to play a major role in Fe cycling have low $\delta^{56}Fe$ values, generally between $-1.0\permil$ and $-3.0\permil$ (Fig. 4). In addition, ferric hydroxides in the same sediments also have relatively low $\delta^{56}Fe$ values, averaging ~$-1.0\permil$ (Fig. 4). Severmann et al. (2006) interpreted the negative $\delta^{56}Fe$ values for reactive Fe(III) oxides to reflect complete or near-complete oxidation of low $\delta^{56}Fe$ $Fe(II)_{aq}$ upon interaction with O_2-bearing seawater, where the low $\delta^{56}Fe$ values for porewater Fe(II) were generated by DIRB deeper in the sediment column. A similar interpretation has been made by Staubwasser et al. (2006) to explain moderately negative $\delta^{56}Fe$ values for reactive Fe(III) oxides in modern sediments from the Arabian Sea. Based on the similarly negative $\delta^{56}Fe$ values for the Navajo oxide concretions, and the inferred low $\delta^{56}Fe$ values for $Fe(II)_{aq}$, we infer that bacterial Fe(III) reduction, coupled with hydrocarbon oxidation, was the major mechanism for mobilizing Fe in the Navajo Sandstone.

Other Mechanisms for Producing Low $\delta^{56}Fe$ Values

It is unknown if low $\delta^{56}Fe$ values for $Fe(II)_{aq}$ may be produced through abiotic reduction of early diagenetic Fe(III) oxides by hydrocarbons.

Experimental studies by Shebl and Surdam (1996) demonstrated increases in porosity in oxide-bearing sandstone during heating (200–360 °C) in the presence of hydrocarbons, but these increases largely occurred through dissolution of carbonate cement, and there were no clear increases in $Fe(II)_{aq}$ contents during reaction. At the lower temperatures (<100 °C) estimated to have characterized Fe mobilization in the Navajo Sandstone, we would expect less reaction between hydrocarbons and sandstone cements. In addition, abiological reduction of Fe(III) oxides coupled with oxidation of organic matter was not observed in experiments run as high as 120 °C at circumneutral pH (Lovley et al., 1991). Therefore, our preferred interpretation is that the role of hydrocarbons in Fe mobilization in the Navajo Sandstone was primarily to serve as an organic carbon source for bacterial Fe(III) reduction rather than as an abiological reductant.

Finally, we consider the possibility that the oxide concretions may reflect in situ oxidation of pyrite concretions. Because many sedimentary pyrites in modern (Severmann et al., 2006) and ancient (Rouxel et al., 2005; Yamaguchi et al., 2005; Archer and Vance, 2006) environments have negative $\delta^{56}Fe$ values, in situ oxidation of pyrite might explain the low $\delta^{56}Fe$ oxide concretions. Such an explanation, however, is unlikely for several reasons. First, pyrite is rarely found in unbleached Navajo Sandstone, and only in trace abundances within bleached sandstones. There is no evidence of any remnant pyrite minerals in the numerous samples of Navajo concretions that have been examined, and if pyrite was important in the diagenetic history, some remnants would be expected. Furthermore, the Navajo Sandstone does not contain any evidence for sulfate minerals, nor is it rich in organic carbon, as is common in pyrite-bearing sedimentary rocks. Second, the widespread distribution, variety, abundance, and geometries of the Navajo concretions are very different from the features observed in pyrite-bearing sedimentary rocks, where pyrite is commonly localized within bedding and/or mineralization along fault zones. More importantly, the distribution of the Fe oxide concretions in the Navajo Sandstone is along geographically extensive redox fronts that are characterized by bleached zone boundaries that cut across primary structures. These features are not consistent with in situ oxidation of pyrite.

A Conceptual Model

We illustrate a conceptual model of redox cycling of Fe and formation of Fe oxide concretions in Figure 5. The $\delta^{56}Fe$ values for the initial, early diagenetic Fe oxides should have been
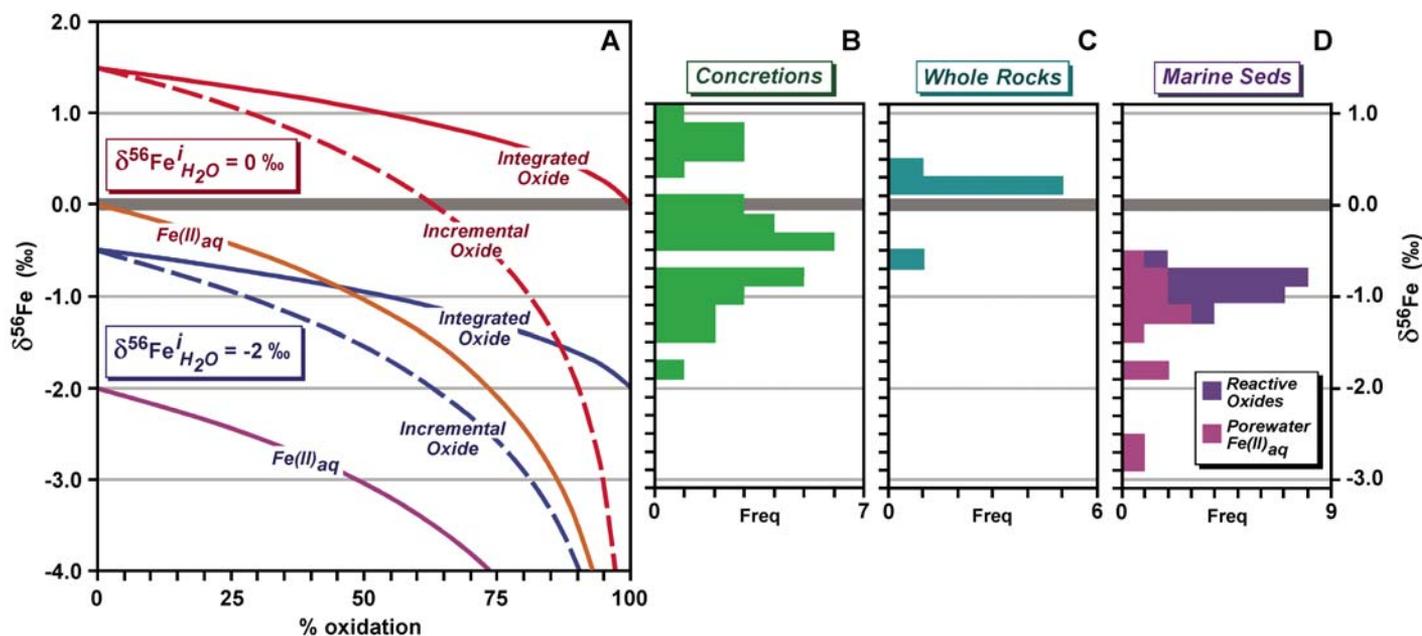
Figure 4. Comparison of $\delta^{56}Fe$ values produced for oxides during oxidation of $Fe(II)_{aq}$ (A) and histograms for $\delta^{56}Fe$ values measured for oxide concretions (B), whole-rock sandstones (C), and reactive $Fe(III)$ oxides and $Fe(II)$-bearing pore waters from modern marine sediments (D). In A, $\delta^{56}Fe$ values were calculated using a Rayleigh model as a function of percent oxidation of $Fe(II)_{aq}$ for the reaction $Fe(II)_{aq} \rightarrow Fe(III)_{aq} \rightarrow Fe(III)$ oxide; once oxidized, 100% of the $Fe(III)_{aq}$ is assumed to precipitate as oxides, which is appropriate for the circum-neutral pH conditions in which the concretions formed. Upper curves (warm colors) illustrate Fe isotope compositions produced for $Fe(II)_{aq}$ that had initial $\delta^{56}Fe = 0.0‰$; lower curves (cool colors) were calculated for an initial $\delta^{56}Fe$ value for $Fe(II)_{aq}$ of −2.0‰. Data for B and C are from Table DR1 (see text footnote 1). Data for D are from modern marine sediments from the California margin (Severmann et al., 2006); $\delta^{56}Fe$ values for reactive $Fe(III)$ oxides were estimated from acid extractions that produced $Fe(III)/Fe_{total} > 0.3$. Porewater compositions are shown for suboxic, low-S samples where dissimilatory $Fe(III)$-reducing bacteria (DIRB) play a major role in Fe cycling. Thick gray line at $\delta^{56}Fe = 0$ notes average of igneous rocks and low-C, low-S clastic sedimentary rocks and weathering products. Thin gray lines were added for scale reference across the figures.
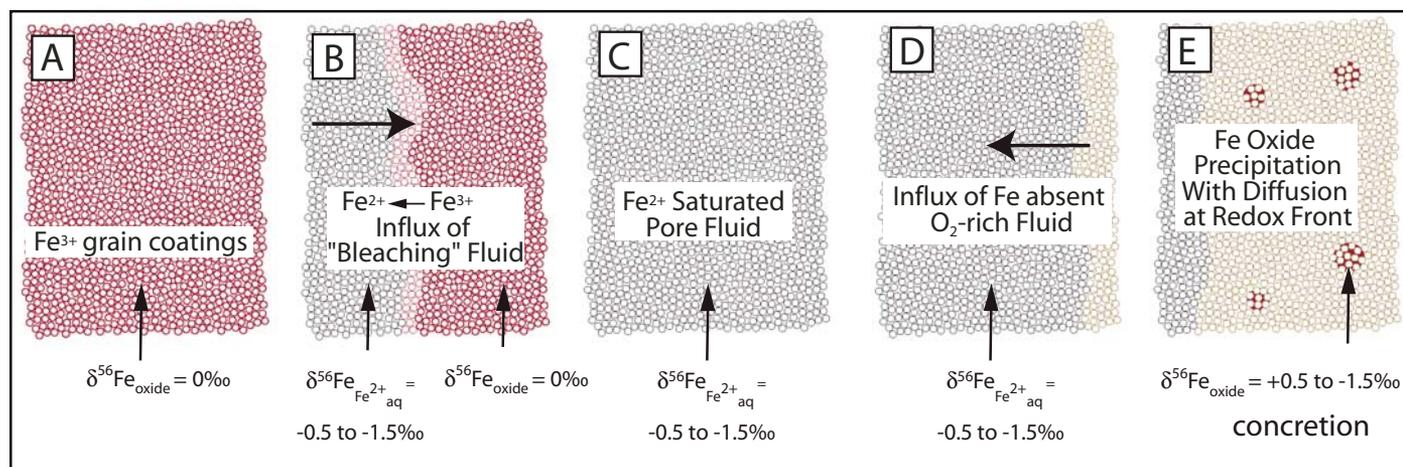

Figure 5. Conceptual grain-scale model of isotopic analyses for stages of redox reactions for Fe cycling in terrestrial examples of Navajo Sandstone concretion formation. (A) Early hematite (Fe^{3+}) grain coatings in original red sandstone, where initial $\delta^{56}Fe = 0.0‰$. (B) Influx of reducing fluids that "bleach" the buried sandstone during reduction of Fe^{3+} to Fe^{2+}, where the $Fe(II)$-rich fluids have $\delta^{56}Fe$ values between −0.5‰ and −1.5‰, probably reflecting bacterial Fe reduction. (C) Bleached sandstone pores are saturated with waters containing reduced iron (Fe^{2+}). (D) Influx of oxidizing groundwater creates redox front where concretions precipitate. (E) Concretions form along a reaction front with organized distribution and spherical shape, producing a range of $\delta^{56}Fe$ values that are generally negative, reflecting complete oxidation and precipitation of low $\delta^{56}Fe$ $Fe(II)_{aq}$.

close to zero (Fig. 5A), as shown by our measurements of Fe oxide in unbleached Navajo sandstone and an extensive database for modern and ancient Fe(III)-rich weathering products. Iron mobilization through incongruent dissolution of the early diagenetic Fe oxides produced Fe(II)$_{aq}$ that has low δ^{56}Fe values of ~−0.5‰ to ~−1.5‰ (Fig. 5B). On average, ~30% Fe reduction occurred based on the contrast in Fe contents between red and bleached whole-rock samples. However, the proportion of mobilized Fe that was eventually sequestered as oxide concretions is difficult to constrain. Field measurements of this proportion are complicated by the highly nonuniform distribution of the oxide concretions, which likely resulted from the superposition of multiple reaction zones of variable scales (from centimeter to kilometer scales and greater) that migrated spatially and/or operated repeatedly over time.

Reductive dissolution most likely occurred by DIRB, where oxide reduction was coupled to hydrocarbon oxidation under anoxic conditions. Reduced, Fe(II)-bearing fluids were transported away from the site of initial oxide reduction (Fig. 5C), where anoxic conditions were likely maintained by dissolved organic carbon. Fe(II)-rich fluids encountered O$_2$-bearing fluids either though ascent of reduced fluids or downward penetration of oxidizing fluids or both (Fig. 5D), which resulted in rapid and complete oxidation and precipitation of Fe(II)$_{aq}$ to ferric oxides and hydroxides at the mixing interface between these fluids. The distribution and size of oxide concretions indicate a major control by nucleation, suggesting that precipitation was rapid. Such a process should produce δ^{56}Fe values for oxide concretions that are generally reflective of the δ^{56}Fe values for the precursor Fe(II)$_{aq}$ (Fig. 5E), although isotopic zoning would be expected due to local (centimeter-scale) changes in δ^{56}Fe values imposed on the remaining Fe(II)$_{aq}$ that existed between nuclei during the oxidation process and final precipitation of the remaining Fe.

Removal of low δ^{56}Fe Fe(II)$_{aq}$ should have produced high δ^{56}Fe values for bleached rocks, but this is not uniformly observed. The δ^{56}Fe values for whole-rock samples of bleached rocks range from −0.16‰ to +0.24‰ (Table DR1, see footnote 1). It is important to note, however, that it is difficult to estimate the δ^{56}Fe value of the Fe inventory that was removed, given the fact that the oxide concretions represent only a small fraction of the Fe that was removed from the bleached zones. Moreover, the lowest δ^{56}Fe values for Fe(II)$_{aq}$ generated by reductive dissolution of Fe oxides by DIRB would be produced only at low extents of reduction (a few percent) (Johnson et al., 2005; Crosby et al., 2005), which

would produce negligible changes in the δ^{56}Fe values of the remaining Fe oxide. It is therefore difficult to calculate a rigorous isotopic mass balance with the current data set, although this may be possible through much more extensive studies of the bleached zones.

CONCLUSIONS

Iron isotope compositions of oxide concretions in the Navajo Sandstone document reductive dissolution of early diagenetic oxides, aqueous transport, and finally precipitation in an open groundwater terrestrial system. Although the mineralogy and inferred fluid chemistry of the Navajo concretions have some important differences from Mars concretions, Fe isotopes should be similarly valuable in constraining Fe pathways and open- or closed-system behavior. In the Navajo system, the generally low δ^{56}Fe values of the oxide concretions point to initial Fe mobilization through incongruent reductive dissolution of early sandstone oxides, probably by dissimilatory Fe(III)-reducing bacteria producing Fe(II)$_{aq}$ with δ^{56}Fe < 0. In the Meridiani Planum system, Fe mobilization is thought to have occurred by acid sulfate weathering of primary silicate minerals in basaltic rock, and in this case, if the fluid reservoir was limited and large extents of dissolution occurred, the δ^{56}Fe values of the fluid would probably lie closer to those of the original basalt, which would be within 0.1‰ of the δ^{56}Fe value of terrestrial basalts (Poitrasson et al., 2004).

Precipitation of aqueous Fe in the Navajo Sandstone probably occurred when reduced groundwaters intersected O$_2$-bearing fluids, and the extent of isotopic fractionation was dependent upon the extent of precipitation that occurred in an open system. Two of the 15 concretions analyzed have δ^{56}Fe > 0, and partial precipitation must have occurred in an open fluid-flow system. However, 13 of the 15 concretions have δ^{56}Fe < 0, which indicates that complete or near-complete precipitation occurred, largely preserving the low δ^{56}Fe values of the fluid. Isotopic zonation within individual concretions would be expected in both terrestrial and Martian systems if local changes (centimeter scale) occurred in fluid composition between nuclei during oxidation and precipitation. In the Meridiani Planum system, where the inferred low pH is expected to have produced significant pools of coexisting aqueous Fe(III) and Fe(II) (Tosca et al., 2005), we might expect only partial precipitation to occur, which would tend to produce oxide concretions that had higher δ^{56}Fe values, similar to the few high δ^{56}Fe concretions found in the Navajo Sandstone.

REFERENCES CITED

Albarède, F., and Beard, B., 2004, Analytical methods for non-traditional isotopes, *in* Johnson, C., Beard, B., and Albarède, F., eds., Geochemistry of Non-Traditional Stable Isotopes: Reviews in Mineralogy and Geochemistry, v. 55, p. 113–152.

Archer, C., and Vance, D., 2006, Coupled Fe and S isotope evidence for Archean microbial Fe(III) and sulfate reduction: Geology, v. 34, p. 153–156, doi: 10.1130/G22067.1.

Balci, N., Bullen, T.D., Witte-Lien, K., Shanks, W.C., Motelica, M., and Mandernack, K.W., 2006, Iron isotope fractionation during microbially stimulated Fe(II) oxidation and Fe(III) precipitation: Geochimica et Cosmochimica Acta, v. 70, p. 622–639, doi: 10.1016/j.gca.2005.09.025.

Beard, B., and Johnson, C., 2004, Chapter 10A: Fe isotope variations in the modern and ancient Earth and other planetary bodies, *in* Johnson, C., Beard, B., and Albarède, F., eds., Geochemistry of Non-Traditional Stable Isotopes: Reviews in Mineralogy and Geochemistry, v. 55, p. 319–357.

Beard, B.L., Johnson, C.M., Cox, L., Sun, H., and Nealson, K.H., 1999, Iron isotope biosignatures: Science, v. 285, p. 1889–1892, doi: 10.1126/science.285.5435.1889.

Beard, B.L., Johnson, C.M., Skulan, J.L., Nealson, K.H., Cox, L., and Sun, H., 2003a, Application of Fe isotopes to tracing the geochemical and biological cycling of Fe: Chemical Geology, v. 195, p. 87–117, doi: 10.1016/S0009–2541(02)00390-X.

Beard, B.L., Johnson, C.M., von Damm, K.L., and Poulson, R.L., 2003b, Iron isotope constraints on Fe cycling and mass balance in oxygenated Earth oceans: Geology, v. 31, p. 629–632, doi: 10.1130/0091–7613(2003)031<0629:IICOFC>2.0.CO;2.

Beitler, B., Parry, W.T., and Chan, M.A., 2003, Bleaching of Jurassic Navajo Sandstone on Colorado Plateau Laramide highs: Evidence of exhumed hydrocarbon supergiants?: Geology, v. 31, p. 1041–1044, doi: 10.1130/G19794.1.

Beitler, B., Parry, W.T., and Chan, M.A., 2005, Fingerprints of fluid flow: Chemical diagenetic history of the Jurassic Navajo Sandstone, southern Utah: Journal of Sedimentary Research, v. 75, p. 547–561, doi: 10.2110/jsr.2005.045.

Berquist, B.A., and Boyle, E.A., 2006, Iron isotopes in the Amazon River system: weathering and transport signatures: Earth and Planetary Science Letters, v. 248, p. 54–68.

Brantley, S.L., Liermann, L., and Bullen, T., 2001, Fractionation of Fe isotopes by soil microbes and organic acids: Geology, v. 29, p. 535–538, doi: 10.1130/0091–7613(2001)029<0535:FOFIBS>2.0.CO;2.

Brantley, S.L., Guynn, R.L., Liermann, L.J., Anbar, A., Barling, J., and Icopini, G., 2004, Fe isotopic fractionation during mineral dissolution with and without bacteria: Geochimica et Cosmochimica Acta, v. 68, p. 3189–3204, doi: 10.1016/j.gca.2004.01.023.

Bullen, T.D., White, A.F., Childs, C.W., Vivit, D.V., and Schultz, M.S., 2001, Demonstration of significant abiotic iron isotope fractionation in nature: Geology, v. 29,

p. 699–702, doi: 10.1130/0091–7613(2001)029<0699: DOSAII>2.0.CO;2.

Busigny, V., and Dauphas, N., 2006, Iron Isotopes in spherical hematite and goethite concretions from the Navajo Sandstone (Utah, USA): A prospective study for "Martian Blueberries": League City, Texas, 37th Annual Lunar and Planetary Science Conference, abstract no. 1200.

Chan, M.A., and Parry, W.T., 2002, Rainbow of Rocks: Mysteries of sandstone colors and concretions in Colorado Plateau Canyon Country: Utah Geological Survey Public Information Series 77, 17 p.

Chan, M.A., Parry, W.T., and Bowman, J.R., 2000, Diagenetic hematite and manganese oxides and fault-related fluid flow in Jurassic sandstones, southeastern Utah: American Association of Petroleum Geologists Bulletin, v. 84, p. 1281–1310.

Chan, M.A., Parry, W.T., Petersen, E.U., and Hall, C.M., 2001, $^{40}Ar-^{39}Ar$ age and chemistry of manganese mineralization in the Moab to Lisbon fault systems, southeastern Utah: Geology, v. 29, p. 331–334, doi: 10.1130/0091–7613(2001)029<0331:AAAACO>2.0.CO;2.

Chan, M.A., Beitler, B., Parry, W.T., Ormö, J., and Komatsu, G., 2004, A possible terrestrial analogue for hematite concretions on Mars: Nature, v. 429, p. 731–734, doi: 10.1038/nature02600, doi: 10.1038/nature02600.

Chan, M.A., Beitler Bowen, B., Parry, W.T., Ormö, J., and Komatsu, G., 2005, Red rock and red planet diagenesis: Comparisons of Earth and Mars concretions: GSA Today, v. 15, no. 8, p. 4–10, doi: 10.1130/1052–5173(2005)015[4:RRARPD]2.0.CO;2.

Christensen, P.R., Wyatt, M.B., Glotch, T.D., Rogers, A.D., Anwar, S., Arvidson, R.E., Bandfield, J.L., Blany, D.L., Budney, C., Calvin, W.M., Fallacaro, A., Fergason, R.L., Gorelick, N., Graff, T.G., Hamilton, V.E., Hayes, A.G., Johnson, J.R., Knudson, A.T., McSween, H.Y., Jr., Mehall, G.L., Mahall, L.K., Moersch, J.E., Morris, R.V., Smith, M.D., Squyres, S.W., Ruff, S.W., and Wolff, M.J., 2004, Mineralogy at Meridiani Planum from the mini-TES experiment on the *Opportunity* rover: Science, v. 306, p. 1733–1739, doi: 10.1126/science.1104909.

Cordova, R.M., 1978, Ground-water conditions in the Navajo Sandstone in the central Virgin River basin, Utah: Utah Department of Natural Resources Technical Publication, v. 61, p. 1978.

Croal, L.R., Johnson, C.M., Beard, B.L., and Newman, D.K., 2004, Iron isotope fractionation by Fe(II)-oxidizing photoautotrophic bacteria: Geochimica et Cosmochimica Acta, v. 68, p. 1227–1242, doi: 10.1016/j.gca.2003.09.011.

Crosby, H.A., Johnson, C.M., Roden, E.E., and Beard, B.L., 2005, Coupled Fe(II)-Fe(III) electron and atom exchange as a mechanism for Fe isotope fractionation during dissimilatory iron oxide reduction: Environmental Science & Technology, v. 39, p. 6698–6704, doi: 10.1021/es0505346, doi: 10.1021/es0505346.

Dauphas, N., and Rouxel, O., 2006, Mass spectrometry and natural variations of iron isotopes: Mass Spectrometry Reviews, v. 25, p. 515–550, doi: 10.1002/mas.20078.

Dumitru, T.A., Duddy, I.R., and Green, P.F., 1994, Mesozoic-Cenozoic burial, uplift, and erosion history of the west-central Colorado Plateau: Geology, v. 22, p. 499–502, doi: 10.1130/0091–7613(1994)022<0499: MCBUAE>2.3.CO;2.

Herkenhoff, K.E., Squyres, S.W., Arvidson, R., Bass, D.S., Bell, J.F., III, Bertelsen, P., Cabrol, N.A., Gaddis, L., Hayes, A.G., Hviid, S.F., Johnson, J.R., Kinch, K.M., Madsen, M.B., Maki, J.N., McLennan, S.M., McSween, H.Y., Rice, J.W., Jr., Sims, M., Smith, P.H., Soderblom, L.A., Spanovich, N., Sullivan, R., and Wang, A., 2004, Evidence from *Opportunity*'s microscopic imager for water on Meridiani Planum: Science, v. 306, p. 1727–1730, doi: 10.1126/science.1105286.

Icopini, G.A., Anbar, A.D., Ruebush, S.S., Tien, M., and Brantley, S.L., 2004, Iron isotope fractionation during microbial reduction of iron: The importance of adsorption: Geology, v. 32, p. 205–208, doi: 10.1130/G20184.1.

Jeon, B.H., Dempsey, B.A., Burgos, W.D., and Royer, R.A., 2001, Reactions of ferrous iron with hematite: Colloids and surfaces—A: Physicochemical Engineering Aspects, v. 191, p. 41–55, doi: 10.1016/S0927-7757(01)00762-2.

Johnson, C.M., and Beard, B.L., 2005, Biogeochemical cycling of iron isotopes: Science, v. 309, p. 1025–1027, doi: 10.1126/science.1112552, doi: 10.1126/science.1112552.

Johnson, C.M., and Beard, B.L., 2006, Stable isotope geochemistry of transitional elements provides new insights into biogeochemical cycles: Examples from the Fe isotope system: GSA Today, v. 16, no. 11, p. 4–10, doi: 10.1130/GSAT01611A.1.

Johnson, C.M., Skulan, J.L., Beard, B.L., Sun, H., Nealson, K.H., and Braterman, P.S., 2002, Isotopic fractionation between Fe(III) and Fe(II) in aqueous solutions: Earth and Planetary Science Letters, v. 195, p. 141–153, doi: 10.1016/S0012–821X(01)00581–7.

Johnson, C.M., Beard, B., Roden, E., Newman, D., and Nealson, K., 2004, Chapter 10B: Isotopic constraints on biogeochemical cycling of Fe, *in* Johnson, C., Beard, B., and Albarède, F., eds., Geochemistry of Non-Traditional Stable Isotopes: Reviews in Mineralogy and Geochemistry, v. 55, p. 359–408.

Johnson, C.M., Roden, E.E., Welch, S.A., and Beard, B.L., 2005, Experimental constraints on Fe isotope fractionation during magnetite and Fe carbonate formation coupled to dissimilatory hydrous ferric oxide reduction: Geochimica et Cosmochimica Acta, v. 69, p. 963–993.

Lindquist, S.J., 1988, Practical characterization of eolian reservoirs for development: Nugget Sandstone, Utah Wyoming thrust belt: Sedimentary Geology, v. 56, p. 315–339, doi: 10.1016/0037-0738(88)90059-0.

Lovley, D.R., Phillips, E.J., and Lonergan, D.J., 1991, Enzymatic versus nonenzymatic mechanisms for Fe(III) reduction in aquatic sediments: Environmental Science & Technology, v. 25, p. 1062–1067, doi: 10.1021/es00018a007.

McLennan, S.M., Bell, J.F., III, Calvin, W., Christensen, P.R., Clark, B.C., de Souza, P.A., Farmer, J., Farrand, W.H., Fike, D.A., Gellert, R., Ghosh, A., Glotch, T.D., Grotzinger, J.P., Hahn, B., Herkenhoff, K.E., Hurowitz, J.A., Johnson, J.R., Johnson, S.S., Jolliff, B.L., Klingelhöfer, G., Knoll, A.H., Learner, Z.A., Malin, M.C., McSween, H.Y., Jr., Pocock, J., Ruff, S.W., Soderblom, L.A., Squyres, S.W., Tosca, N.J., Watters, W.A., Wyatt, M.B., and Yen, A., 2005, Provenance and diagenesis of the evaporite-bearing Burns formation, Meridiani Planum, Mars: Earth and Planetary Science Letters, v. 240, p. 95–121, doi: 10.1016/j.epsl.2005.09.041.

Morris, R.V., Ming, D.W., Graff, T.G., Arvidson, R.E., Bell, J.F., III, Squyres, S.W., Mertzman, S.A., Gruener, J.E., Golden, D.C., Le, L., and Robinson, G.A., 2005, Hematite spherules in basaltic tephra altered under aqueous, acid sulfate conditions on Mauna Kea volcano, Hawaii: Possible clues for the occurrence of hematite-rich spherules in the Burns formation at Meridiani Planum, Mars: Earth and Planetary Science Letters, v. 240, p. 168–178, doi: 10.1016/j.epsl.2005.09.044.

Nealson, K., and Saffarini, D., 1994, Iron and manganese in anaerobic respiration: Environmental significance, physiology and regulation: Annual Review of Microbiology, v. 48, p. 311–343, doi: 10.1146/annurev.mi.48.100194.001523.

Nuccio, V.F., and Condon, S.M., 1996, Burial and thermal history of the Paradox basin, Utah and Colorado, and petroleum potential of the Middle Pennsylvanian Paradox Formation: U.S. Geological Survey Bulletin 2000-O, 41 p.

Ormö, J., Komatsu, G., Chan, M.A., Beitler, B., and Parry, W.T., 2004, Geological features indicative of processes related to the hematite formation in Meridiani Planum and Aram Chaos, Mars: A comparison with diagenetic hematite deposits in southern Utah, USA: Icarus, vol. 171, p. 295–316. doi: 10.1016/j.icarus.2004.06.001.

Poitrasson, F., Halliday, A.N., Lee, D.-C., Levasseur, S., and Teutsch, N., 2004, Iron isotope differences between Earth, Moon, Mars and Vesta as possible records of contrasted accretion mechanisms: Earth and Planetary Science Letters, v. 223, p. 253–266, doi: 10.1016/j.epsl.2004.04.032.

Rouxel, O.J., Bekker, A., and Edwards, K.J., 2005, Iron isotope constraints on the Archean and Paleoproterozoic ocean redox state: Science, v. 307, p. 1088–1091, doi: 10.1126/science.1105692.

Seilacher, A., 2001, Concretion morphologies reflecting diagenetic and epigenetic pathways: Sedimentary Geology, v. 143, p. 41–57, doi: 10.1016/S0037–0738(01)00092–6.

Severmann, S., Johnson, C.M., Beard, B.L., and McManus, J., 2006, The effect of early diagenesis on the Fe isotope compositions of pore waters and authigenic minerals in continental margin sediments: Geochimica et Cosmochimica Acta, v. 70, p. 2006–2002.

Shebl, M.A., and Surdam, R.C., 1996, Redox reactions in hydrocarbon clastic reservoirs: Experimental validation of this mechanism for porosity enhancement: Chemical Geology, v. 132, p. 103–117.

Squyres, S.W., Grotzinger, J.P., Arvidson, R.E., Bell, J.F., III, Calvin, W., Christensen, P.R., Clark, B.C., Crisp, J.A., Farrand, W.H., Kerkenhoff, K.E., Johnson, J.R., Klingelhöfer, G., Knoll, A.H., McLennan, S.M., McSween, H.Y., Jr., Morris, R.V., Rice, J.W., Jr., Rieder, R., and Soderblom, L.A., 2004, In situ evidence for an ancient aqueous environment at Meridiani Planum, Mars: Science, v. 306, p. 1709–1714, doi: 10.1126/science.1104559.

Staubwasser, M., von Blanckenburg, F., and Schoenberg, R., 2006, Iron isotopes in the early marine diagenetic iron cycle: Geology, v. 34, p. 629–632, doi: 10.1130/G22647.1.

Teutsch, N., Von Gunten, U., Porcelli, D., Cirpka, O.A., and Halliday, A.N., 2005, Adsorption as a cause for iron isotope fractionation in reduced groundwater: Geochimica et Cosmochimica Acta, v. 69, p. 4175–4185, doi: 10.1016/j.gca.2005.04.007.

Tosca, N.J., McLennan, S.M., Clark, B.C., Grotzinger, J.P., Hurowitz, J.A., Knoll, A.H., Schröder, C., and Squyres, S.W., 2005, Geochemical modeling of evaporation processes on Mars: Insight from the sedimentary record at Meridiani Planum: Earth and Planetary Science Letters, v. 240, no. 1, p. 122–148, doi: 10.1016/j.epsl.2005.09.042.

Von Gunten, U., and Schneider, W., 1991, Primary products of the oxygenation of iron (II) at an oxic-anoxic boundary: Nucleation, aggregation, and aging: Journal of Colloid and Interface Science, v. 145, p. 127–139, doi: 10.1016/0021–9797(91)90106-I.

Welch, S.A., Beard, B.L., Johnson, C.M., and Braterman, P.S., 2003, Kinetic and equilibrium Fe isotope fractionation between aqueous Fe(II) and Fe(III): Geochimica et Cosmochimica Acta, v. 67, p. 4231–4250, doi: 10.1016/S0016-7037(03)00266-7.

Yamaguchi, K.E., Johnson, C.M., Beard, B.L., and Ohmoto, H., 2005, Biogeochemical cycling of iron in the Archean-Paleoproterozoic Earth: Constraints from iron isotope variations in sedimentary rocks from the Kaapvaal and Pilbara cratons: Chemical Geology, Special Issue on Isotopic Biosignatures, v. 218, p. 135–169, doi: 10.1016/j.chemgeo.2005.01.020.